Sea Ice Mapping from Compact Polarimetric SAR Imagery Using Contextual Information and Learned Features

Saeid Taleghanidoozdoozan — University of Waterloo
Linlin Xu — University of Waterloo
David A.Clausi — University of Waterloo
Email: stalegha@uwaterloo.ca

Abstract

The RADARSAT Constellation Mission (RCM) offers a compact polarimetric (CP) synthetic aperture RADAR (SAR) mode that provides a wider swath than quad-polarization (QP) and more polarization information in observations than dual-polarization (DP). We investigate the capability of CP SAR imagery in generating sea ice maps by taking advantages of learned features, statistical properties, and contextual information. We present a region-based sea ice mapping methodology. First, an existing unsupervised segmentation called iterative region growing with semantics based on statistical properties of CP SAR data (CP-IRGS) is used to generate edge-preserved and homogeneous regions to reduce destructive effects of speckle noise. Then, a residual-based convolutional neural network (ResCNN) is used to specify the type of ice in regions. The performance of the proposed classification methodology is compared to that of standard machine learning classifiers, support vector machine (SVM) and random forest (RF). To simulate CP SAR data, two QP RADARSAT-2 scenes are utilized. The obtained results indicate that the proposed region-based classification methodology achieves 96.66% overall accuracy, which is approximately 4% higher than those obtained by SVM and RF.

1 Introduction

Accurate sea ice mapping from synthetic aperture radar (SAR) images is critical to support various applications such as climate change and northern ocean navigation [1, 2]. The RADARSAT constellation mission (RCM), as Canada's newest generation of Earth observation SAR satellites, consists of three satellites operating in single-polarization, dual-polarization (DP), compact polarimetric (CP), and quad-polarization (QP) acquisition modes [3]. The coherency matrix of CP SAR data is a 2×2 semi-positive definite Hermitian matrix. For a hybrid-polarity mode [4] in which a right circular polarized wave (R) is transmitted and coherent dual linear horizontal (H) and vertical (V) polarizations are received, the coherency matrix is given as:

$$\mathbf{C}_{CP} = \begin{bmatrix} \langle | S_{RH}^2 | \rangle & \langle S_{RH} S_{RV}^* \rangle \\ \langle S_{RV} S_{RH}^* \rangle & \langle | S_{RV}^2 | \rangle \end{bmatrix} \tag{1}$$

where $\langle ... \rangle$ and * indicate spatial ensemble averaging and the conjugate transpose, respectively. S_{ij} is a complex-valued element in which i and j show transmitted and received polarizations, respectively [5].

There are limited publications that assess CP SAR data for sea ice mapping, such as [6–8]. The previous studies used standard machine learning methods such as support vector machine (SVM) [9] or random forest (RF) [10] to generate sea ice maps while feature learning methods such as convolutional neural networks (CNNs) have shown promising performance in ocean applications [11–14]. Moreover, in the previous studies, statistical properties of CP SAR data were not considered in generating sea ice maps.

Therefore, to address the above mentioned limitations, in this paper, a region-based sea ice classification in CP SAR imagery is proposed in which learned features, statistical characteristics and contextual information in CP SAR imagery are utilized. First an existing unsupervised segmentation method called iterative region growing with semantics based on statistical properties of CP SAR data (CP-IRGS) [15] is used to segment CP SAR data into edge-preserved and homogeneous regions. Then, a residual-based CNN (ResCNN) classifier is designed to specify the ice-type labels for each region.

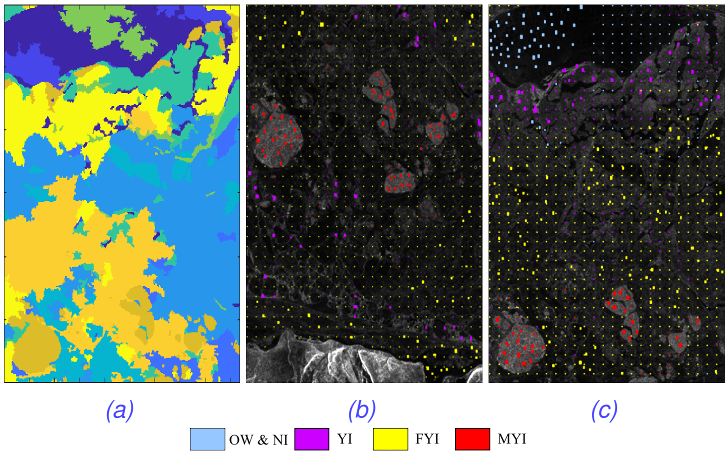

Fig. 1: (a) CP-IRGS output using the simulated CP data. (b) Training and (c) Test scenes along with labeled pixels.

Table 1: The number of training and testing pixels for each class.

Name	Description	# of train	# of test
OW/NI	open water and new ice	2000	3290
YI	young ice	5889	6383
FYI	first-year ice	6396	6383
MYI	multi-year ice	5750	5714

2 Experiments

2.1 Study Area

Due to the limited available CP SAR data, a popular method to obtain CP SAR data is to simulate them using QP SAR data. In this study, two RADARSAT-2 scenes are used to simulate CP SAR data [16]. Fig. 1 shows the study area which includes five different classes: young ice (YI), first-year ice (FYI), multi-year ice (MYI), new ice (NI), and open water (OW) identified by experts in the Canadian Ice Service (CIS). Since the backscatter signatures of OW and NI classes are similar in the test scene, they are assumed as the same class (OW/NI).

The number of labeled pixels specified by CIS experts is approximately 1000, which were used to guide the collection of the remaining labeled pixels. Table 1 shows the number of training and test pixels in each class. Since the training scene does not include sufficient numbers of OW/NI samples, 2000 OW/NI samples are obtained from the test scene to train models.

2.2 Results and Discussion

Table 2 shows the structure of the designed ResCNN model which it is trained by minimizing the multi-class cross-entropy lost function [17]. To minimize the loss function, the Adam optimizer [18] is employed. After training the ResCNN model, all pixels in a CP SAR image can be classified to obtain pixel-level sea ice maps. As inputs for training the ResCNN model, 3×17×17 patches (3 channels as the absolute value of the coherency matrix elements) are extracted around each labeled pixel. However, the number of training patches in each class is not equal known as unbalanced problem. To overcome this unbalanced problem, the data augmentation technique, including horizontal and vertical flips as well as random rotation, is used to expand the number of training patches to 7000 per each class.

Table 2: Structure of the ResCNN model along with the operators.

Layer name	Output Size	Operators
Block 1	$17 \times 17 \times 16$	$\begin{bmatrix} 3 \times 3 \times 16 \\ 3 \times 3 \times 16 \end{bmatrix}$
Block 2	$9 \times 9 \times 32$	$\begin{bmatrix} 3 \times 3 \times 32 \\ 3 \times 3 \times 32 \end{bmatrix}$
Block 3	$5 \times 5 \times 48$	$\begin{bmatrix} 3 \times 3 \times 48 \\ 3 \times 3 \times 48 \end{bmatrix}$
Block 4	$3 \times 3 \times 64$	$\begin{bmatrix} 3 \times 3 \times 64 \\ 3 \times 3 \times 64 \end{bmatrix}$
Global Average	$1 \times 1 \times 64$	3×3 average pool
Classification	4	64×4 fully connected
Softmax	4	

Table 3: Confusion matrices obtained by the ResCNN model and the baseline approaches using the simulated CP.

Method		OW/NI	YI	FYI	MYI	User's Accuracy(%)
RF	OW/NI	**3263**	18	6	77	96.99
	YI	3	**4742**	1037	630	73.95
	FYI	24	563	**5305**	2	90.00
	MYI	0	1060	35	**5005**	82.05
	Overall Accuracy (%):					84.13
	Kappa Coefficient:					0.7847
SVM	OW/NI	**3259**	21	9	77	96.82
	YI	1	**4714**	1110	370	76.09
	FYI	30	460	**5227**	3	91.38
	MYI	0	1188	37	**5264**	81.12
	Overall Accuracy (%):					84.81
	Kappa Coefficient:					0.7942
ResCNN	OW/NI	**3287**	40	3	69	96.70
	YI	1	**4393**	615	139	85.33
	FYI	2	733	**5761**	13	88.50
	MYI	0	1217	4	**5493**	81.81
	Overall Accuracy (%):					**86.97**
	Kappa Coefficient:					**0.8235**

Table 4: Confusion matrices obtained by the region-based sea ice classification methodology using the simulated CP as well as the two baseline RF, SVM classifiers.

Method		OW/NI	YI	FYI	MYI	User's Accuracy(%)
SVM+CP-IRGS	OW/NI	**3284**	7	2	59	97.97
	YI	3	**4980**	120	21	97.19
	FYI	3	22	**6257**	6	99.51
	MYI	0	1374	4	**5628**	80.33
	Overall Accuracy (%):					92.55
	Kappa Coefficient:					0.8991
RF+CP-IRGS	OW/NI	**3284**	8	2	59	97.94
	YI	3	**4977**	120	20	97.21
	FYI	3	22	**6257**	6	99.51
	MYI	0	1376	4	**5629**	80.31
	Overall Accuracy (%):					92.54
	Kappa Coefficient:					0.8990
ResCNN+CP-IRGS	OW/NI	**3284**	32	1	43	97.74
	YI	3	**5874**	121	24	97.54
	FYI	3	23	**6259**	22	99.24
	MYI	0	454	2	**5625**	92.50
	Overall Accuracy (%):					**96.66**
	Kappa Coefficient:					**0.9546**

Fig. 2 (a)-(c) show the pixel-level sea ice maps generated by RF, SVM and the ResCNN model and the corresponding confusion matrix is shown in Table 3. The overall accuracy (OA) obtained by

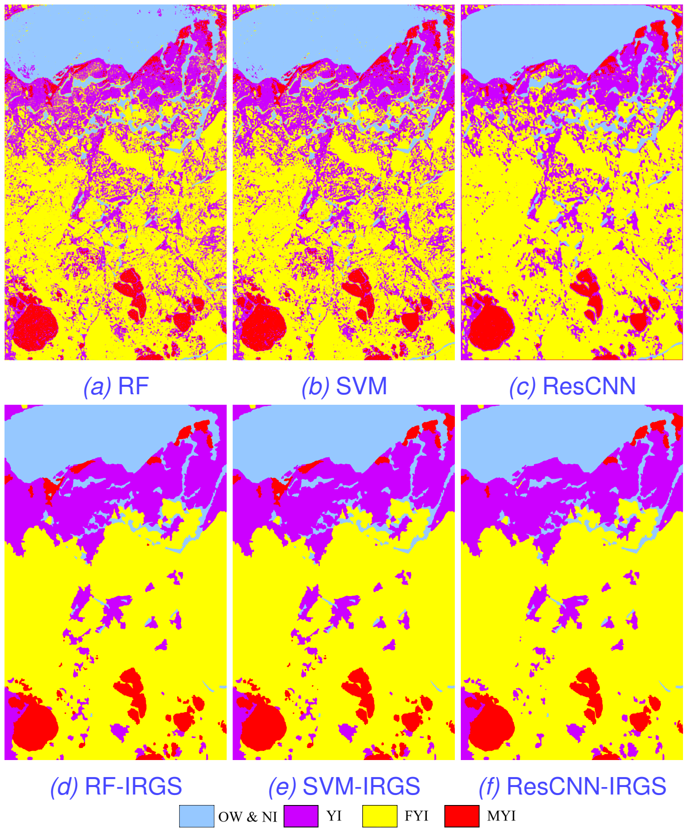

Fig. 2: (a)-(c) Sea ice maps generated by the RF, SVM, and the designed CNN model. (d)-(f) Obtained sea ice maps by combining the regions generated by CP-IRGS with the pixel-level classified scenes by applying a majority voting in each region.

the ResCNN model is approximately 2% higher than those obtained by RF and SVM. Compared to the ResCNN model, the results obtained by SVM and RF are noisier, and OA values confirm it. In general, all models have detected many YI pixels in the upper part of the scene as MYI. It could be because the intensity values of those YI pixels are close to those of MYI pixels. Overall, all three maps appear quite noisy because many small within-class artifacts are identified. These small artifacts may be better removed by leveraging contextual information in the CP-IRGS segmentation algorithm. Moreover, the areas around edges tend to have a high rate of misclassification, which may be improved by combining with regions generated by CP-IRGS.

The final results are achieved by combining the pixel-level sea ice maps with the homogeneous regions (Fig. 2 (d)-(f)). In general, compared to the pixel-level sea ice maps (Fig. 2 (a)-(c)), the final results provide well-identified homogeneous areas, and less noisy effect caused by small artifacts. According to Table 4, integrating the output of the ResCNN model and the regions (ResCNN+CP-IRGS) achieves 96.66% OA. This demonstrates that CP SAR data has reliable potential for sea ice mapping by using the region-based sea ice classification methodology. Combining the outputs of RF and SVM with the homogeneous regions (RF+CP-IRGS and SVM+CP-IRGS) achieve 92.55% OA which is approximately 4% lower than that obtained by ResCNN+CP-IRGS, indicating that using deep learning models instead of standard machine learning classifiers can significantly increase the accuracy of sea ice maps using CP SAR imagery.

3 Conclusion

This paper has presented a methodology based on high-level and contextual information on SAR imagery to classify different ice types. At first, a four-block residual-based CNN model is designed to utilize high-level features to reach a high accuracy labeled map. Although the ResCNN model reached high accurate sea ice map, the labeled map was noisy, and some edges vanished. Therefore, homogeneous regions were extracted from the CP SAR image using the CP-IRGS segmentation method which it considers the statistical characteristics of CP SAR data and preserves edges among different objects. Combining the labeled map with regions by applying a majority voting increased OA.

To do more investigation on the performance of the region-based classification methodology, two popular traditional machine learning classification methods, namely, SVM and RF, were used. These methods benefit from feature engineering and low-level information. SVM and RF reached OA=84.81% and OA=84.13%, respectively. However, combining the outputs of SVM and RF with CP-IRGS generated regions reached a higher accuracy of OA=92.54% and OA=92.55% which in comparison with OA obtained by the ResCNN+CP-IRGS model, they are approximately 4% lower.

Although the region-based classification methodology is used for generating sea ice maps, it has considerable potential for addressing other tasks such as land cover identification. Moreover, it does not consider the dependency among pixels which can be considered in future works.

References

[1] D. G. Barber, "Microwave remote sensing, sea ice and Arctic climate," *Phys. Can*, vol. 61, pp. 105–111, 2005.

[2] D. N. Thomas, *Sea ice*. John Wiley & Sons, 2017.

[3] F. Charbonneau, M. Arkett, B. Brisco, J. Buckley, H. Chen, D. Goodenough, C. Liu, H. McNarin, J. Poitevin, J. Shang *et al.*, "Meeting canadian user needs with the radarsat constellation mission's compact polarimetry mode: A summary assessment," *Ottawa. Geomatics Canada Open File*, no. 34, 2017.

[4] R. K. Raney, "Hybrid-polarity SAR architecture," *IEEE Transactions on Geoscience and Remote Sensing*, vol. 45, no. 11, pp. 3397–3404, 2007.

[5] J.-S. Lee and E. Pottier, *Polarimetric radar imaging: from basics to applications*. CRC press, 2009.

[6] S. Singha and R. Ressel, "Arctic sea ice characterization using risat-1 compact-pol SAR imagery and feature evaluation: A case study over northeast greenland," *IEEE Journal of Selected Topics in Applied Earth Observations and Remote Sensing*, vol. 10, no. 8, pp. 3504–3514, 2017.

[7] M. Ghanbari, D. A. Clausi, L. Xu, and M. Jiang, "Contextual classification of sea-ice types using compact polarimetric SAR data," *IEEE Transactions on Geoscience and Remote Sensing*, vol. 57, no. 10, pp. 7476–7491, 2019.

[8] M. Dabboor, B. Montpetit, and S. Howell, "Assessment of the high resolution SAR mode of the RADARSAT constellation mission for first year ice and multiyear ice characterization," *Remote Sensing*, vol. 10, no. 4, p. 594, 2018.

[9] C. Cortes and V. Vapnik, "Support-vector networks machine learning (pp. 237–297), vol. 20," 1995.

[10] T. K. Ho, "Random decision forests," in *Proceedings of 3rd international conference on document analysis and recognition*, vol. 1. IEEE, 1995, pp. 278–282.

[11] H. Lyu, W. Huang, and M. Mahdianpari, "Eastern arctic sea ice sensing: First results from the RADARSAT Constellation Mission data," *Remote Sensing*, vol. 14, no. 5, p. 1165, 2022.

[12] S. Khaleghian, H. Ullah, T. Kræmer, N. Hughes, T. Eltoft, and A. Marinoni, "Sea ice classification of SAR imagery based on convolution neural networks," *Remote Sensing*, vol. 13, no. 9, p. 1734, 2021.

[13] Y. Han, Y. Liu, Z. Hong, Y. Zhang, S. Yang, and J. Wang, "Sea ice image classification based on heterogeneous data fusion and deep learning," *Remote Sensing*, vol. 13, no. 4, p. 592, 2021.

[14] Y. Huang, Y. Ren, and X. Li, "Classifying sea ice types from SAR images using a U-Net-based deep learning model," in *2021 IEEE International Geoscience and Remote Sensing Symposium IGARSS*. IEEE, 2021, pp. 3502–3505.

[15] M. Ghanbari, D. A. Clausi, and L. Xu, "CP-IRGS: A region-based segmentation of multilook complex compact polarimetric SAR data," *IEEE Journal of Selected Topics in Applied Earth Observations and Remote Sensing*, vol. 14, pp. 6559–6571, 2021.

[16] F. Charbonneau, B. Brisco, R. Raney, H. McNairn, C. Liu, P. Vachon, J. Shang, R. DeAbreu, C. Champagne, A. Merzouki *et al.*, "Compact polarimetry overview and applications assessment," *Canadian Journal of Remote Sensing*, vol. 36, no. sup2, pp. S298–S315, 2010.

[17] A. Bahri, S. G. Majelan, S. Mohammadi, M. Noori, and K. Mohammadi, "Remote sensing image classification via improved cross-entropy loss and transfer learning strategy based on deep convolutional neural networks," *IEEE Geoscience and Remote Sensing Letters*, vol. 17, no. 6, pp. 1087–1091, 2019.

[18] D. P. Kingma and J. Ba, "Adam: A method for stochastic optimization," *arXiv preprint arXiv:1412.6980*, 2014.